Volume 14
Number 23
17 June 2026
Pages 7069–7390

Journal of Materials Chemistry B

Materials for biology and medicine

rsc.li/materials-b

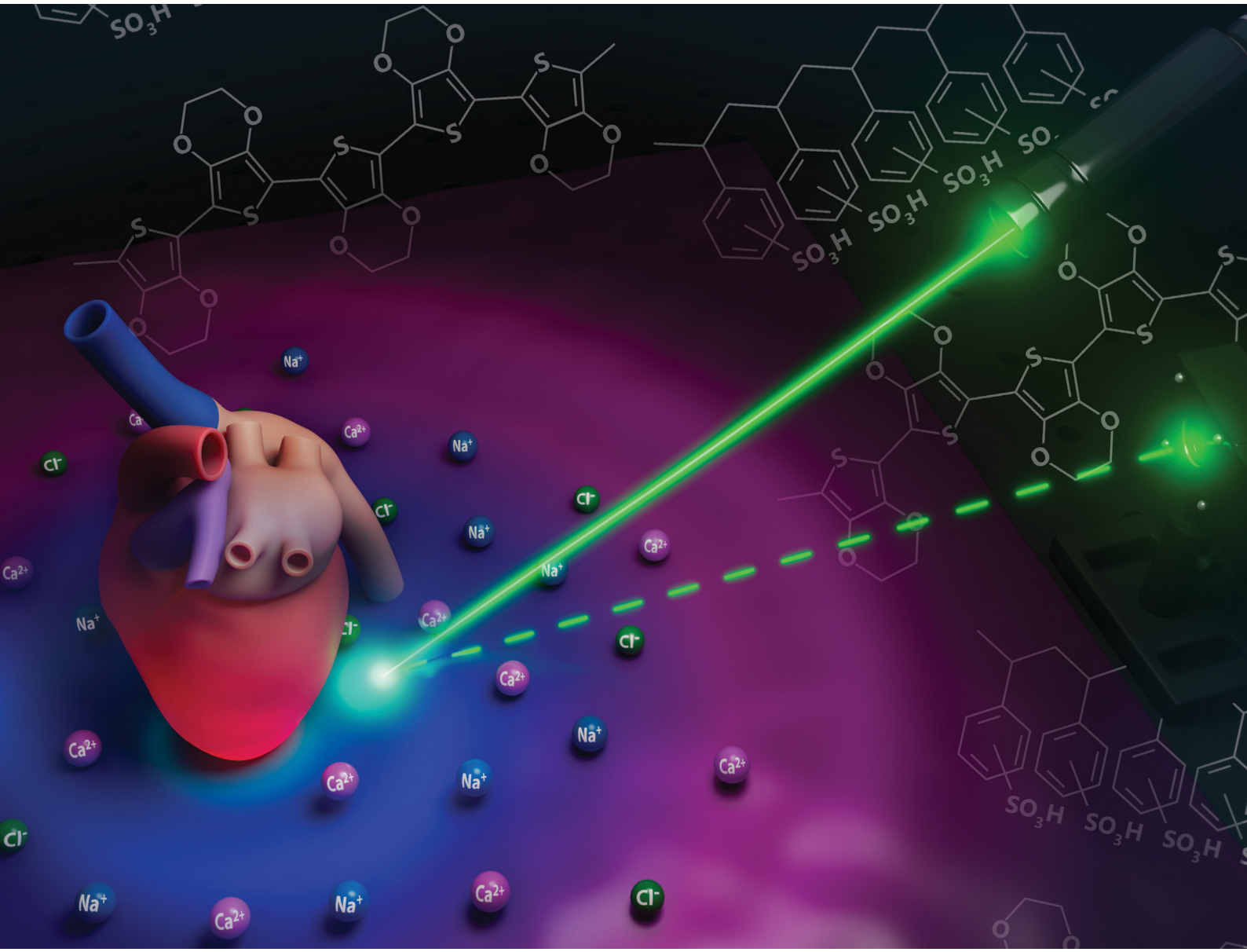

ISSN 2050-750X

ROYAL SOCIETY OF CHEMISTRY

PAPER

Yuecheng Peter Zhou *et al.*

Controlling PEDOT:PSS electropolymerization for label-free optical recording of bioelectric potentials

Journal of Materials Chemistry B

ROYAL SOCIETY OF CHEMISTRY

PAPER

View Article Online
View Journal | View Issue

Cite this: J. Mater. Chem. B, 2026, 14, 7150

Controlling PEDOT:PSS electropolymerization for label-free optical recording of bioelectric potentials

Xuchen Ren,†[a] Jitong Ren,†[b] Yu Shi,[c] Alexandra Kuhlman-Schneider,[a] Koney Eungkon Kim,[a] Zixin Zhang[a] and Yuecheng Peter Zhou *[abdef]

Label-free optical recording of bioelectric potentials provides a non-perturbative approach for detecting bioelectric activities. Electrochromic materials, such as PEDOT:PSS, change their optical absorbance under external voltages. The voltage-dependent absorbance change allows recording of bioelectric potentials without using fluorescent reporters, and does not suffer from photobleaching or phototoxicity. Nevertheless, the voltage recording sensitivity of PEDOT:PSS strongly depends on its electrochromic properties. Here, we investigated how electropolymerization conditions of PEDOT:PSS thin films, including counterions, pH, PSS molecular weight, and substrate surface treatment, influence their electrochromic response. We found counterion competition is the dominant factor: introducing Cl^- as a competing counterion in addition to PSS during PEDOT electropolymerization blue-shifts the $\pi-\pi^*$ absorption peaks by ~120 nm, alters film morphology and electrochromic response, and enhances optical anisotropy. At the same time, it reduces the voltage-dependent absorbance change at shorter (blue-green) wavelengths while enhancing it at longer (red) wavelengths. Using PEDOT:PSS thin films electropolymerized without Cl^- and a 561 nm laser, we achieved a voltage detection sensitivity of 2.8 μV at 10 kHz recording bandwidth under shot-noise-limited conditions. We then performed prolonged label-free optical recording of isolated embryonic chicken hearts. We recorded both the cardiac field potentials and mechanical contractions, which increased from embryonic day 10 to day 15, while the latency time between them remained unchanged. These results established electropolymerization as a strategy to tune the electrochromic response of PEDOT:PSS thin films across different wavelengths, thereby optimizing their voltage detection sensitivity.

Received 8th April 2026,
Accepted 1st May 2026

DOI: 10.1039/d6tb00816j

rsc.li/materials-b

Introduction

Bioelectric signals arise from the coordinated activity of ion channels in electrogenic cells such as neurons and cardiomyocytes. They underpin a wide range of physiological functions, including neuronal communication and cardiac contraction.[1,2]

[a] Department of Materials Science and Engineering, The Grainger College of Engineering, University of Illinois Urbana-Champaign, Urbana, IL, USA. E-mail: zhou62@illinois.edu
[b] Department of Chemical and Biomolecular Engineering, College of Liberal Arts & Sciences, University of Illinois Urbana-Champaign, Urbana, IL, USA
[c] Department of Chemistry, College of Liberal Arts & Sciences, University of Illinois Urbana-Champaign, Urbana, IL, USA
[d] Department of Bioengineering, The Grainger College of Engineering, University of Illinois Urbana-Champaign, Urbana, IL, USA
[e] Materials Research Laboratory, University of Illinois Urbana-Champaign, Urbana, IL, USA
[f] Beckman Institute for Advanced Science and Technology, University of Illinois Urbana-Champaign, Urbana, IL, USA
† Equal contributions.

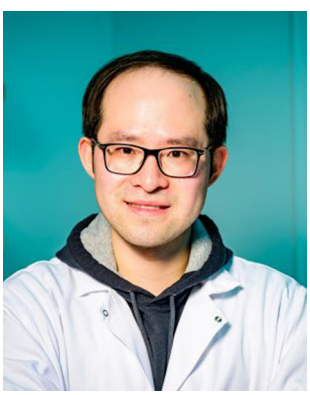

Yuecheng Peter Zhou

Dr Yuecheng "Peter" Zhou is an Assistant Professor of Materials Science and Engineering at the University of Illinois Urbana-Champaign, with affiliated appointments in Bioengineering, Chemical and Biomolecular Engineering, Materials Research Laboratory and Beckman Institute for Advanced Science and Technology. Dr Zhou received his BS and PhD in Materials Science and Engineering from the University of Illinois Urbana-Champaign, followed by postdoctoral training at Stanford University Department of Chemistry and Wu Tsai Neurosciences Institute. The Zhou lab works at the intersection of materials science, optics, and biology to investigate bioelectric and biochemical cues in the heart and brain.

Reliable detection of bioelectric activities is essential for understanding cell functions,[3] diagnosing diseases,[4,5] and developing bioelectronic interfaces.[6–8] In recent years, optical detection of bioelectric signals has emerged as a powerful approach. It offers high spatial resolution, the flexibility to record from arbitrary cells, and the capability for wide-field voltage imaging.[9] Current optical recording approaches typically rely on inserting voltage-sensitive fluorescent reporters into the cell membrane to convert bioelectric signals into optical readouts.[10,11] Genetically-encoded voltage indicators offer unique advantages such as selective expression in a desired cell type for *in vivo* voltage imaging.[12] However, these probes exhibit reduced contrast and brightness when imaging at high frame rates (*e.g.*, 0.5–1 kHz). Under such conditions, recording durations are typically limited to seconds to minutes due to photobleaching and phototoxicity.[13,14]

Label-free optical recording approaches have been developed to overcome these limitations associated with fluorescent voltage reporters.[15] The key to label-free optical recording is to convert bioelectric signals into a stable optical readout without using fluorescent reporters. Among these approaches, electrochromic optical recording (ECORE) leverages the electrochromic properties of π-conjugated polymers, such as poly(3,4-ethylenedioxythiophene) poly(styrenesulfonate) (PEDOT:PSS), to convert bioelectric signals into an optical absorbance change.[16–18] By measuring the absorbance (reflectance) change of the polymer film outside the cells or tissue, ECORE allows stable and sensitive optical recording of bioelectric signals in a label-free and non-perturbative manner. It does not suffer from photobleaching and allows us to use much lower laser power than that needed to excite fluorescence molecules.

The sensitivity of ECORE scales positively with the electrochromic contrast of PEDOT:PSS. Therefore, controlling the synthesis of PEDOT:PSS to maximize its electrochromic contrast, and elucidating its structure–property relationships, is crucial for further improving the ECORE detection sensitivity. PEDOT:PSS thin films can be electrochemically synthesized by oxidation of 3,4-ethylenedioxythiophene (EDOT) monomers under an applied potential or current, known as electropolymerization. Oxidation of the EDOT monomer generates radical cation intermediates that can be stabilized in a protonated form. Coupling between two such activated species forms a dimer, followed by deprotonation to initiate the growth of positively charged PEDOT chains.[19]

Electropolymerization of EDOT monomers in the presence of negatively-charged counterions stabilizes the positive charges on the PEDOT chains. Using water-soluble counterions such as PSS, electropolymerization enables the formation of PEDOT:PSS thin films on electrode surfaces from aqueous solutions under well-defined electrochemical conditions.[20] This approach is widely used to reduce electrical impedance, owing to the mixed electronic-ionic conductivity of PEDOT:PSS,[21] while also improving biocompatibility for electrode-based recordings of bioelectric potentials.[22–25] For this reason, previous studies have largely focused on controlling the structure and electrical properties of PEDOT films modulated by pH[26] or counterions[23] *via* electropolymerization. Few studies have focused on its electrochromic properties.[27]

Here, we use electropolymerization to tune the electrochromic responses of PEDOT:PSS thin films for ECORE. Electropolymerization offers a convenient way to control film properties through multiple deposition parameters while keeping the same PEDOT:PSS materials framework. We systematically investigated how electropolymerization conditions, including counterions, pH, PSS molecular weight and substrate surfaces, influence their electrochromic properties. We found that among these factors, counterions play a dominant role in regulating the electrochromic contrast of PEDOT:PSS thin films. While past studies have largely relied on using a single counterion for PEDOT spectral tuning,[23,27,28] we found by introducing a secondary competing counterion, Cl^-, in addition to PSS during EDOT electropolymerization, the structure, electrochemical response, and electrochromic contrast of PEDOT:PSS thin films can all be precisely controlled.

Using this approach, we maximized the electrochromic contrast of PEDOT:PSS at targeted wavelengths to enhance the ECORE detection sensitivity. Using a 561 nm laser, we achieved a detection sensitivity of 2.8 μV at 10 kHz recording bandwidth. We performed prolonged label-free optical recording of both the field potential and mechanical contraction of isolated embryonic chicken hearts at day 10 and 15, and revealed how these signals evolve during embryonic chicken heart development. With the capability of tuning PEDOT:PSS electrochromic contrast, we are no longer restricted by specific probing wavelengths. This flexibility opens opportunities to employ alternative wavelengths for ECORE and couple it with other imaging modalities.

Results

Control PEDOT:PSS thin film electrochromic response through electropolymerization

PEDOT:PSS consists of conductive PEDOT-rich domains electrostatically complexed with a PSS polyanion matrix.[29–31] The structure of PEDOT:PSS is strongly influenced by the electrostatic interactions formed during electropolymerization. We investigated parameters perturbing such interactions, including competing counterion concentration, pH, PSS molecular weight, and substrate surface properties (Fig. 1a). As illustrated in Fig. 1b, PEDOT:PSS thin films were synthesized when a constant current was applied to an indium–tin–oxide (ITO) glass serving as a working electrode, with a platinum wire serving as a counter electrode and an Ag/AgCl electrode serving as the reference electrode. We found the dominant factor controlling the electrochromic response of PEDOT:PSS thin films is the competition between counterions during electropolymerization. Prior work has shown that incorporating single counterions during EDOT electropolymerization could alter the Vis-NIR spectroelectrochemistry of PEDOT films.[32] However, for optical recording of bioelectric signals, the counterions associated with PEDOT must be biocompatible. We found, by simply introducing NaCl, the predominant salt in extracellular biological fluids, during PEDOT:PSS electropolymerization, Cl^- acts as a competing small counterion (as opposed to polymer counterion PSS). It can alter the charge compensation between

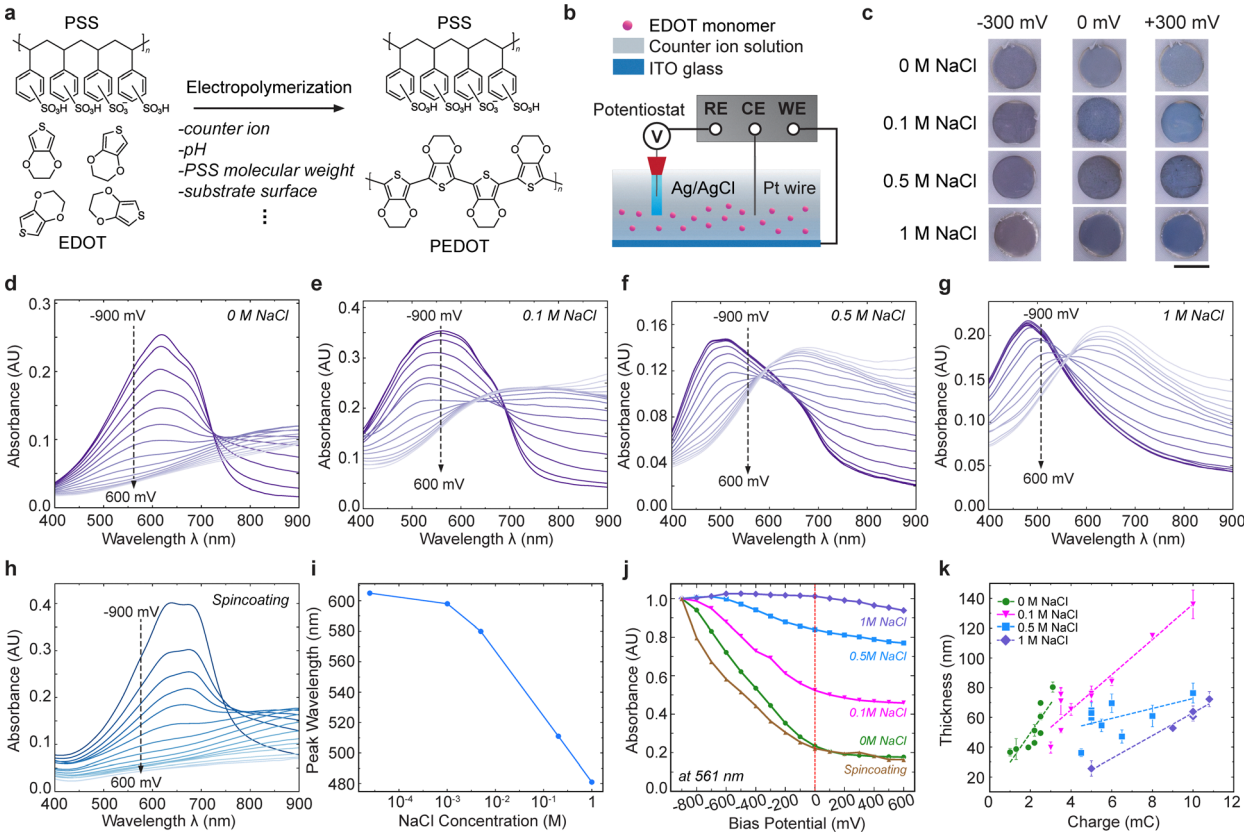

Fig. 1 Spectral tuning of PEDOT:PSS thin films *via* electropolymerization. (a) Synthesizing PEDOT:PSS thin films *via* electropolymerization of EDOT in the presence of PSS, with counterions, electrolyte pH, PSS molecular weight, and substrate surface conditions as key parameters. (b) Three-electrode setup with ITO glass working electrode (WE), Pt counter electrode (CE), and Ag/AgCl reference electrode (RE). (c) Color change of PEDOT:PSS thin films prepared under different NaCl concentrations at −300 mV, 0 mV, and +300 mV. Scale bar = 5 mm. Visible-near infrared (Vis-NIR) spectroelectrochemistry of PEDOT:PSS thin films electropolymerized with (d) 0 M, (e) 0.1 M, (f) 0.5 M, and (g) 1 M NaCl from −900 mV to +600 mV in HEPES-buffered Tyrode's salt solution *versus* Ag/AgCl reference electrode. (h) Vis-NIR spectroelectrochemistry of spin-coated PEDOT:PSS film from −900 mV to +600 mV. (i) Peak absorption wavelength as a function of NaCl concentration. (j) Normalized vis-NIR absorbance change of PEDOT:PSS thin films electropolymerized under different NaCl concentrations at 561 nm. The dashed line indicates zero bias potential. (k) Film thickness as a function of accumulated charge during electropolymerization under different NaCl concentrations.

PEDOT and PSS, and influence the film properties. Indeed, ~60 nm PEDOT:PSS thin films electropolymerized under different NaCl concentrations exhibit distinct colors under the same applied potentials at −300 mV, 0 mV and +300 mV with respect to an Ag/AgCl reference electrode in HEPES-buffered Tyrode's solution (Fig. 1c). This indicates tunable electrochromic color shifts through small counterion incorporation.

To quantify the electrochromic behavior of electropolymerized PEDOT:PSS thin films, we measured their visible-near infrared (Vis-NIR) absorption spectra when the applied potential was changed from −900 mV to +600 mV *versus* Ag/AgCl in HEPES-buffered Tyrode's solution (Fig. 1d–g, "Methods"). As a direct comparison, the Vis-NIR absorption spectra of spin-coated PEDOT:PSS thin film from commercialized suspensions ("Methods") under the same applied potential was shown (Fig. 1h). This potential window is sufficient to drive the films between the reduced (de-doped) and oxidized (doped) states. All films show pronounced voltage-dependent spectral shifts and an absorption peak resulting from the π–π* transition in the reduced state (−900 mV). The spin-coated PEDOT:PSS film exhibits an absorption peak at 637 nm, whereas electropolymerized PEDOT films prepared in pure PSS electrolyte show a peak at 604 nm. Introducing NaCl during electropolymerization results in a significant blue shift of peak absorption maxima at 580 nm, 511 nm, and 481 nm under 0.1 M, 0.5 M, and 1 M NaCl concentration, respectively. Fig. 1i shows the peak absorption wavelength monotonically decreases as a function of NaCl concentration with a wavelength shift of ~120 nm. The blue-shifted π–π* peak, together with the polaron and bipolaron transitions in the Vis-NIR absorption spectra, suggests a reduced effective conjugation length and increased localization of charge carriers.[33–37] Electropolymerized PEDOT:PSS thin films also exhibit more localized charge carriers than spin-coated PEDOT:PSS films in general.

Fig. 1j shows the normalized Vis-NIR absorbance change as a function of the applied potential at 561 nm, which is the probing laser wavelength used for ECORE. Distinct electrochromic behaviors are observed for PEDOT:PSS thin films electropolymerized with varying NaCl concentrations. Films electropolymerized without Cl^- counterions exhibit the largest voltage-dependent absorbance change at negative applied potentials and become

comparable to spin-coated PEDOT:PSS thin films at positive potentials. However, spin-coated PEDOT:PSS films contain less electroactive sites than electropolymerized PEDOT:PSS, which positively affects ECORE sensitivity[18] (more details in the next section). At 561 nm, increasing Cl^- concentration suppresses the absorbance change and films electropolymerized with 1 M NaCl shows minimal voltage-dependent absorbance change across the entire potential window. This is consistent with its significantly blue-shifted Vis-NIR spectra (Fig. 1g). The voltage-dependent absorbance changes at other commonly used laser wavelengths differ significantly from those at 561 nm (Fig. S1). These results show that spectral tuning of PEDOT:PSS thin films *via* competing-counterion-regulated electropolymerization can directly modulate their electrochromic contrast at a given probing wavelength. This method provides a framework to better match the electrochromic contrast of PEDOT:PSS thin films at specific probing light wavelengths to optically detect bioelectric signals.

The thickness of PEDOT:PSS thin films increases nearly linearly with accumulated charges up to ~140 nm for all NaCl concentrations (Fig. 1k), which indicates charge-controlled electropolymerization.[38] Here, electropolymerization was carried out under a constant current, such that the accumulated charge is linearly proportional to time. Accordingly, the slope of the linear fit defines the film growth rate. Introducing competing Cl^- counterions slows down the film growth kinetics during electropolymerization. PEDOT:PSS films electropolymerized in the absence of NaCl exhibit the highest apparent growth rate, whereas introducing Cl^- ions leads to significantly reduced thickness at the same accumulated charge. This can be rationalized as counterion competition influences nucleation and growth kinetics during film formation. We conjecture that Cl^- may increase the nucleation density owing to its small size and lead to a higher density of PEDOT domains. However, PSS can act as a polyanion scaffold at the ITO glass surface and spatially confine EDOT nucleation.[39,40] This may reduce nucleation density and favor more vertical film growth that results in thicker films under the same electropolymerization time.

While completing counterion strongly affects the electrochromic properties of electropolymerized PEDOT:PSS thin films, additional parameters were also investigated. When the electrolyte pH shift from 2 to 6, a moderate (~45 nm) blue shift in the π–π* absorption peak position was observed (Fig. S2a). This indicates protonation conditions during film growth influence the electronic structure of the resulting films.[41] We also compared the Vis-NIR absorbance spectra of PEDOT:Cl films (EDOT electropolymerized in 0.1 M NaCl without PSS, Fig. S2b) under different applied voltages with those of electropolymerized PEDOT:PSS films. The PEDOT:Cl film shows a π–π* absorption peak at 475 nm, and its spectroelectrochemistry resembles that of PEDOT:PSS films electropolymerized with 1 M NaCl. In contrast, PSS molecular weight results in minor changes in the π–π* peak position (Fig. S2c). Noticeable differences only appear in the NIR region (700–900 nm) for 15 kDa PSS, where the low-energy absorption tail at reduced states could arise from the structural disorder in the PEDOT:PSS film.[42] Similarly, alternative substrate surface treatment methods (*e.g.*, UV-ozone activation) produces minimal changes in the absorption spectra (SI Text and Fig. S3b).

Structural characterization of electropolymerized PEDOT:PSS thin films

The surface morphology of electropolymerized PEDOT:PSS films was characterized by atomic force microscopy (AFM) (Fig. 2a) to understand the influence of counterion incorporation. Films prepared in the absence of NaCl exhibit large granular domains on the order of 100 nm. The film shows a root-mean-square (RMS) surface roughness of 12.3 nm. Introducing Cl^- during electropolymerization leads to significantly smoother surfaces. As the NaCl concentration increases from 0.1 M to 1 M, the RMS roughness decreases to 6.6 nm, 5.5 nm, and 4.5 nm, respectively. The lateral granular domain size also decreased (48.2 nm, 37.9 nm, 25.9 nm, 26.8 nm, respectively) with increasing NaCl concentration, as quantified by the mean equivalent disk radius obtained from grain analysis using a consistent thresholding criterion (Fig. S4). Two-dimensional fast Fourier transform (2D FFT) analysis of the height maps and the corresponding power spectral density function (PSDF) indicate no pronounced intrinsic in-plane anisotropy across all samples.

We then examined whether these morphological changes are accompanied by variations in chemical composition. We performed X-ray photoelectron spectroscopy (XPS) to determine the surface composition of PEDOT:PSS thin films electropolymerized under different NaCl concentrations. High-resolution Cl 2p spectra (Fig. 2b) show chlorine signals in samples electropolymerized with NaCl. Peak fitting reveals contributions from both chloride anion (Cl^-) and covalently bonded chlorine (C–Cl). This indicates that chlorine atoms are incorporated into the PEDOT:PSS films rather than merely remaining in the electrolyte solution. Quantitative analysis further shows that the Cl/PEDOT ratio increases with NaCl concentration, rising from 0.019 to 0.169 as the NaCl concentration increases from 0.01 M to 1 M (Tables S1 and S2). We further analyzed the S 2p region to examine the relative contributions of PSS and PEDOT in the films (Fig. 2c). The S 2p spectra were deconvoluted into components corresponding to sulfonate sulfur from PSS and thiophene sulfur from PEDOT, together with peaks associated with the oxidized $PEDOT^+$ species. Quantitative fitting indicates that the PSS/PEDOT ratio remains around 1 for all NaCl concentration. This trend suggests that increasing chlorine incorporation during electropolymerization has limited impact on PSS concentration in polymer films – the increasing chlorine content in the film has dominated effects on the spectral shift of PEDOT:PSS thin films. Attenuated total reflectance Fourier transform infrared (ATR-FTIR) spectroscopy measurements further confirmed this trend (Fig. S5).

Next, we examined how structural and compositional changes influence the electrochemical properties of PEDOT:PSS thin films. The electroactive site concentration in each PEDOT:PSS film was calculated from the cathodic charge from the cyclic voltammetry (CV) measurements (Fig. 2d) by integrating the reductive current, assuming each electroactive site corresponds to one electron-transfer event. We found PEDOT:PSS thin films electropolymerized with 0 M and 0.1 M NaCl show the highest

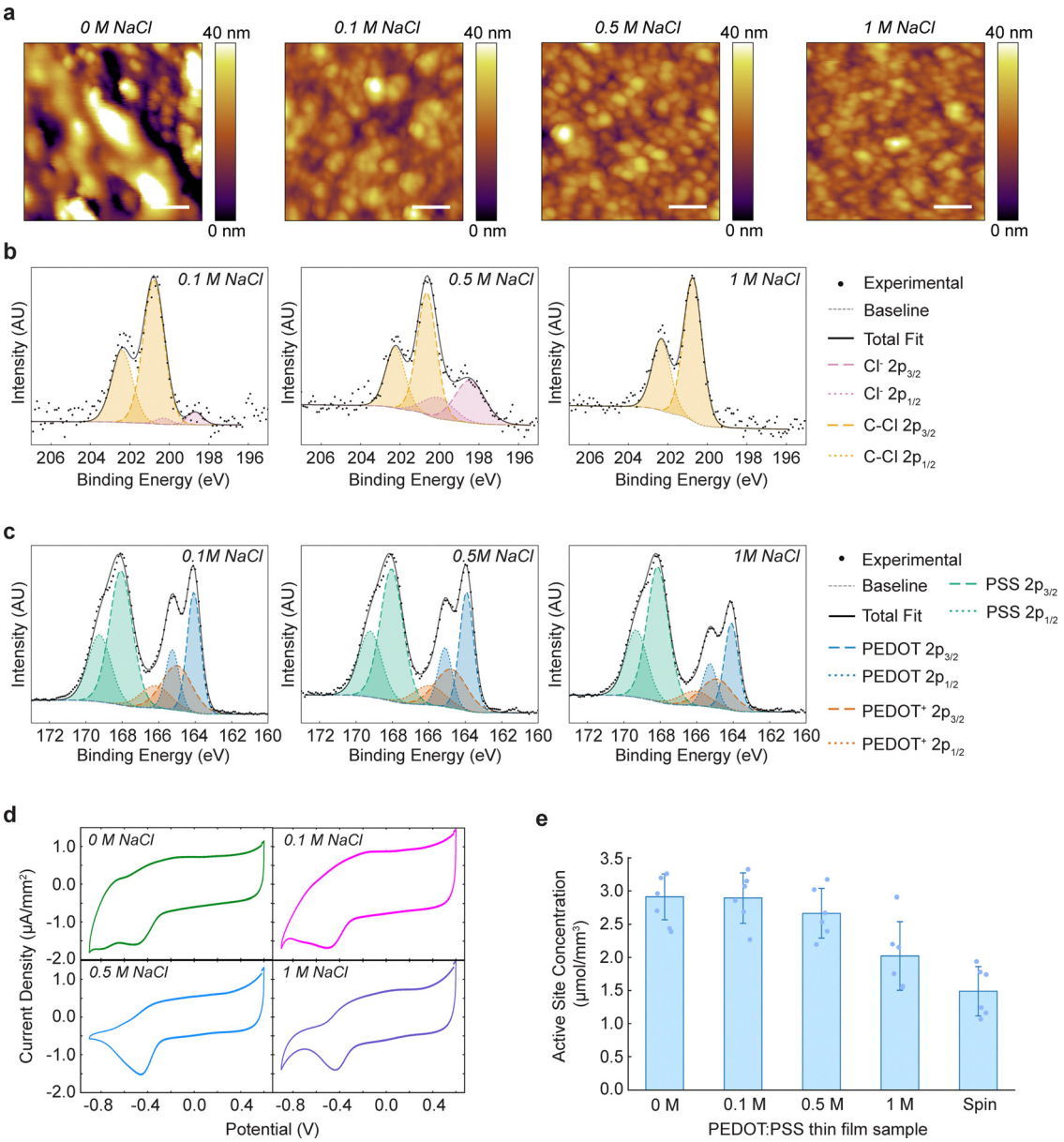

Fig. 2 Structural and electrochemical characterization of electropolymerized PEDOT:PSS thin films. (a) Atomic force microscopy (AFM) images (1×1 μm^2) of PEDOT:PSS films electropolymerized with 0 M, 0.1 M, 0.5 M, and 1 M NaCl. Scale bar = 200 nm. (b) High-resolution Cl 2p XPS spectra of PEDOT:PSS films. (c) High-resolution S 2p XPS spectra of PEDOT:PSS films. (d) Cyclic voltammograms (CVs) of PEDOT:PSS films electropolymerized with 0 M, 0.1 M, 0.5 M, and 1 M NaCl from −900 mV to +600 mV *versus* Ag/AgCl reference electrode in HEPES-buffered Tyrode's solution. (e) Electroactive site concentration calculated from CVs of electropolymerized and spin-coated PEDOT:PSS thin films.

active site concentration of 2.9 ± 0.3 μmol mm^{-3}, and gradually decreases to 2.7 ± 0.4 μmol mm^{-3} and 2 ± 0.5 μmol mm^{-3} for films electropolymerized with 0.5 M and 1 M NaCl, respectively (Fig. 2e). Electropolymerized PEDOT:PSS films also exhibit 30% to 100% higher active site concentrations compared to the spin-coated films (1.5 ± 0.4 μmol mm^{-3}). This may result from the low weight percentage (1.0–1.3 wt%) of the commercial PEDOT:PSS dispersions.[18] These results show that Cl^- incorporation likely alters the electrostatic interaction between PEDOT and PSS that leads to reorganized PEDOT domains[43] and fewer electrochemically accessible redox sites.

ECORE responses of PEDOT:PSS thin films under cell-free conditions

To characterize the performance of PEDOT:PSS thin films electropolymerized under different NaCl in ECORE, we built an optical detection setup based on a prism-coupled total internal reflectance (TIR) configuration and differential photodetection (Fig. 3a), as previously described.[16–18] A linearly polarized 561 nm laser was used as the probing light source and the voltage-induced film reflectance change, ΔR, was recorded when an external potential is applied (Fig. 3b). The ΔR of electropolymerized PEDOT:PSS and PEDOT:Cl thin films

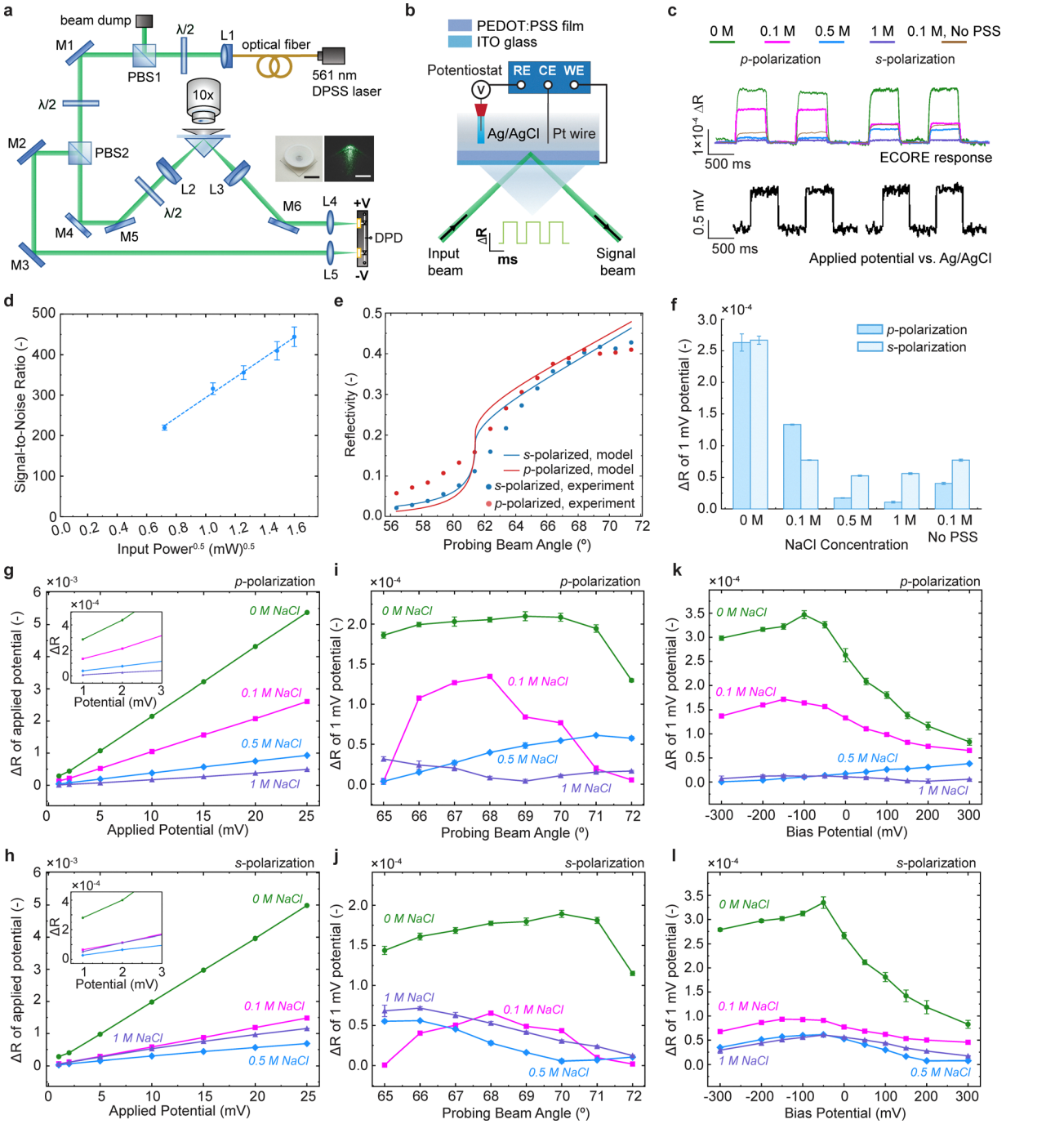

Fig. 3 Characterization of ECORE sensitivity using PEDOT:PSS films electropolymerized under different NaCl concentrations. (a) Optical setup of ECORE. A 561 nm fiber-coupled DPSS laser is directed through a series of mirrors (M), lenses (L), half-wave plates ($\lambda/2$), and polarized beam splitters (PBS). The beam is coupled to the sample using a right-angle prism and is detected using a differential photodetector (DPD). Inset 1: photo of a PEDOT:PSS thin film device for ECORE measurements. Scale bar = 5 mm. Inset 2: focused 561 nm probing laser spot. The image is false colored and scale bar = 100 μm. (b) Schematic of the squarewave experiment. A three-electrode setup with ITO glass working electrode (WE), Ag/AgCl reference electrode (RE), and Pt counter electrode (CE) is used to apply potential on the electropolymerized PEDOT:PSS film. The signal beam is detected to measure the film reflectance change, ΔR, under the applied potentials. (c) Measured reflectance change, ΔR, using *s*- and *p*-polarized light (top panel) when a train of 1 mV, 1 Hz squarewave potential (bottom panel) was applied to PEDOT:PSS films electropolymerized under different NaCl concentrations and PEDOT:Cl films without PSS. (d) Signal-to-noise ratio (SNR) of ΔR in response to 1 mV, 1 Hz squarewave potential as a function of square root input power. Data was measured using *p*-polarized light using electropolymerized PEDOT:PSS film with 0 M NaCl. (e) PEDOT:PSS film reflectance, R, as a function of probing beam incidence angle for *s*-polarized and *p*-polarized light from experiment and modeling. (f) Reflectance change, ΔR, of different electropolymerized PEDOT:PSS and PEDOT:Cl films in response to 1 mV, 1 Hz squarewave potential measured using *s*-polarized and *p*-polarized light at 0 mV bias potential. ΔR, of different electropolymerized PEDOT:PSS films as a function of applied potential measured using (g) *p*-polarized and (h) *s*-polarized light. ΔR, of different electropolymerized PEDOT:PSS films in response to 1 mV, 1 Hz squarewave potential at different probing beam incident angles measured using (i) *p*-polarized and (j) *s*-polarized light, and under different bias potentials measured using (k) *p*-polarized and (l) *s*-polarized light. Data are presented as mean ± SD; $n \geq 40$ squarewave cycles.

under a train of 1 mV, 1 Hz square-wave potential (at 0 mV bias potential) was recorded using both *p*- and *s*-polarized light (Fig. 3c). For PEDOT:PSS films electropolymerized with 0 M NaCl, ΔR responses are comparable when measured using *p*-polarized ($\Delta R = 2.6 \times 10^{-4} \pm 1.4 \times 10^{-5}$) and *s*-polarized light ($\Delta R = 2.7 \times 10^{-4} \pm 6.4 \times 10^{-6}$) (Fig. 3f). Increasing NaCl concentration during electropolymerization leads to a reduction in ΔR for both polarizations, which is consistent with the decreased voltage-dependent Vis-NIR absorbance change at 561 nm (Fig. 1j); it also increases the differences in ΔR recorded using *p*- and *s*-polarized light. At 0.1 M NaCl, ΔR recorded using *p*-polarized light is ~72% higher than recorded using *s*-polarized light. This trend completely reversed for films electropolymerized with 0.5 M and 1 M NaCl, where ΔR recorded with *s*-polarized light is more than twice that obtained with *p*-polarized light. (Fig. 3f).

PEDOT:Cl films electropolymerized with 0.1 M NaCl without PSS show substantially lower ΔR, but a more pronounced polarization dependence compared to PEDOT:PSS film electropolymerized without NaCl. However, compared to the ΔR ($7.7 \times 10^{-5} \pm 1.6 \times 10^{-6}$) of PEDOT:PSS films electropolymerized with 0.1 M NaCl, PEDOT:Cl films electropolymerized under the same NaCl concentration (but without PSS) exhibit nearly identical ΔR ($7.7 \times 10^{-5} \pm 5.4 \times 10^{-7}$) when measured using *s*-polarized light. However, when recorded using *p*-polarized light, the recorded ΔR shows a ~70% reduction, decreasing from $1.3 \times 10^{-4} \pm 8.1 \times 10^{-7}$ to $0.4 \times 10^{-4} \pm 1.6 \times 10^{-6}$.

Since PEDOT:PSS film electropolymerized without NaCl (0 M) shows the highest ΔR response to applied potential using *p*-polarized 561 nm laser, we investigated the ΔR signal-to-noise ratio (SNR) in response to 1 mV, 1 Hz squarewave as a function of the probing laser power. As shown in Fig. 3d, the SNR increases with the square root of the input optical power. This indicates the ECORE system reached shot-noise-limited performance.[44] Using 1.58 mW incident laser power, we achieved an SNR of 356 for 1 mV, 1 Hz applied squarewave potential at 10 kHz recording frequency. This corresponds to a detection sensitivity of 2.8 μV, which improves the previously-reported ~5 μV ECORE sensitivity using PEDOT:PSS thin films[17] by 44%. To determine the incidence angle of the probing laser, we further measured the reflectivity of the PEDOT:PSS film as a function of the incidence angle for both *s*- and *p*-polarized light (Fig. 3e). Experimentally measured reflectivity was fitted using a multilayer reflectivity model (“Methods”). This enables calibration of the optical incidence angle and simultaneously extracting the optical constants of the PEDOT:PSS thin film. The fitting qualitatively captures the film reflectance trend and yields refractive indices $n = 1.49$ and extinction coefficients $\kappa = 0.25$ and 0.22 for *p*- and *s*-polarized light, respectively. The slightly higher κ for *p*-polarized light may result from its greater evanescent field penetration depth and stronger normal electric field component under TIR, leading to increased light absorption. These values fall within previously reported ranges for electropolymerized PEDOT:PSS thin films and the slight discrepancies may result from differences in the polymer Vis-NIR spectra.[17,45,46] For all films measured using *p*- and *s*-polarized light, ΔR increases linearly with the applied squarewave potential over the range of 1–25 mV (Fig. 3g and h). The linear relationship enables quantitative conversion of ΔR to voltage.

Next, we characterized the dependence of the ECORE signal (*i.e.*, ΔR in response to 1 mV, 1 Hz applied potential) on the incidence angle of the probing beam (Fig. 3i and j). A probing beam incident angle dependence was observed for both *p*- and *s*-polarized light. For films electropolymerized with 0 M and 0.1 M NaCl, ΔR initially increases, reaches a maximum at 70° and 68°, respectively, and then decreases. We selected an incidence angle of ~69° for subsequent characterizations. Similar trends were also observed for PEDOT:PSS films (0 M NaCl) with different thicknesses of 39 nm, 61 nm, 80 nm (Fig. S6a and b). This suggests film thickness has negligible contributions to the ECORE signal within the 30–80 nm range, and we used ~60 nm films in this study. For films electropolymerized with 0.5 M NaCl, ΔR keeps increasing with the incidence angle when measured using *p*-polarized light, whereas when measured using *s*-polarized light, it initially decreases, reaching a minimum at 70°, followed by an increase at higher incident angles. For films electropolymerized with 1 M NaCl, the complete opposite was observed – ΔR under *p*-polarized light first decreases and then increases with incident angle (with a turning point at 69°), whereas under *s*-polarized light it decreases monotonically.

To understand the influence of a PEDOT:PSS film redox states on the ECORE signal, we biased the film with different potentials and applied 1 mV, 1 Hz squarewave potential on top of the biasing potential. Consistent with previous findings, ΔR decreases with NaCl concentration during electropolymerization (Fig. 3k and l and Fig. S6c–f). PEDOT:PSS films electropolymerized with 0 M NaCl exhibits the highest ΔR, which first increases, peaks at −100 mV ($\Delta R = 3.5 \times 10^{-4} \pm 8.3 \times 10^{-6}$) when measured using *p*-polarized light and at −50 mV ($\Delta R = 3.3 \times 10^{-4} \pm 1.2 \times 10^{-5}$) when measured using *s*-polarized light before a drastic decrease was observed with bias potential. PEDOT:PSS films electropolymerized with 0.1 M NaCl shows a similar trend. The ΔR reaches a maximum near −150 mV with reduced amplitudes of $1.7 \times 10^{-4} \pm 1.1 \times 10^{-6}$ under *p*-polarized light and $9.3 \times 10^{-5} \pm 6.6 \times 10^{-7}$ under *s*-polarized light. As the NaCl concentration increases, ΔR significantly decreases. For PEDOT:PSS films electropolymerized with 0.5 M and 1 M NaCl, an order of magnitude reduction in ΔR was found compared to films electropolymerized with 0 M NaCl. The dependence of ΔR on the bias potential remains and peaks at −50 mV when measured using *s*-polarized light. However, such a trend was strongly suppressed without any clearly-defined local maximum when measured using *p*-polarized light. The dependence of ΔR on the bias potential for PEDOT:Cl films (0.1 M NaCl, no PSS) resembles that of PEDOT:PSS films electropolymerized with 0.5 M and 1 M NaCl, with slightly higher ΔR when measured using *p*-polarized light. In contrast, when measured using *s*-polarized light, the ΔR dependence on bias potential for PEDOT:Cl shows a similar trend to all PEDOT:PSS thin films, which first increases and then decreases with the applied bias potential. However, instead of peaking at −50 mV as all other PEDOT:PSS films, ΔR peaks between

50 mV and 150 mV for PEDOT:Cl. The ΔR dependence on bias potential for PEDOT:Cl appears nearly as a mirror image of that of PEDOT:PSS electropolymerized with 0.1 M NaCl relative to 0 mV (Fig. S6g and h).

To this end, the dependence of ΔR on probing beam incident angle and bias potential measured using *p*-polarized and *s*-polarized light are similar for PEDOT:PSS thin films electropolymerized at low NaCl concentrations (0 M, 0.1 M). Large divergences in ΔR measured with different laser polarizations emerge for both PEDOT:PSS films electropolymerized with higher NaCl concentrations and PEDOT:Cl films. This behavior suggests that Cl^- incorporation may modify the optical anisotropy of PEDOT thin films, which results in stronger polarization-dependent ΔR, but smaller amplitude due to reduced voltage-dependent absorbance change at 561 nm.

ECORE recording of electric potentials from embryonic chicken hearts

We examined the ECORE performance of recording bioelectric signals from isolated chicken hearts (Fig. 4a). Here, we used PEDOT:PSS thin films electropolymerized with 0 M NaCl and *p*-polarized light as this combination delivers the highest

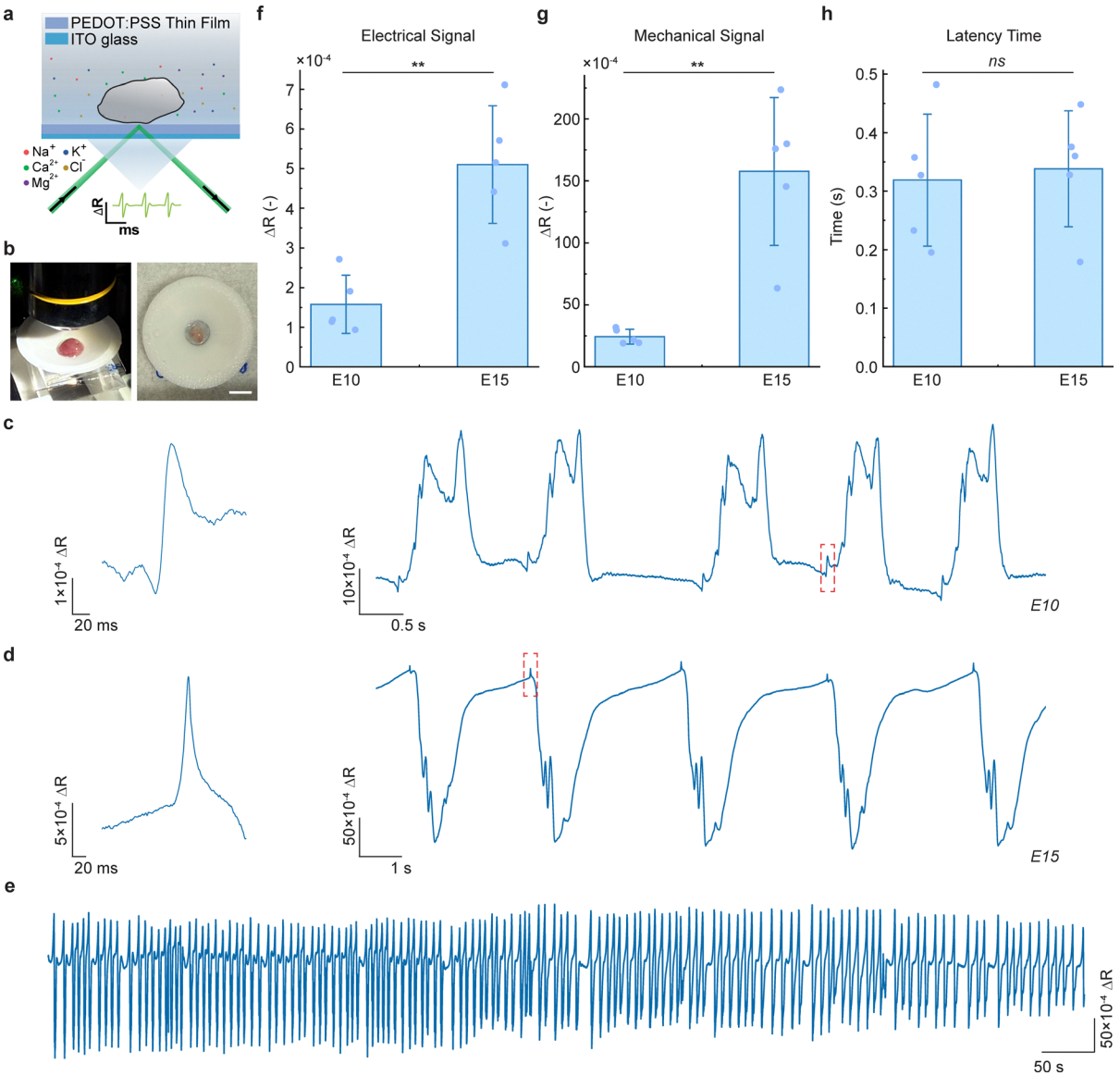

Fig. 4 ECORE recording of isolated chicken heart using PEDOT:PSS thin films. (a) Schematic illustration of an isolated chicken heart interfaced with PEDOT:PSS thin films. The probing laser is focused at the heart-polymer interface and is totally-internally reflected. (b) Photographs of the experimental setup and chicken heart sample used for ECORE measurements. Scale bar = 5 mm. Reflectance change, ΔR, from (c) E10 and (d) E15 chicken hearts, exhibiting periodic activities. The zoomed-in view (red dashed box) shows field potential spikes before mechanical contractions. (e) Representitive 10 min ECORE recording trace from an isolated E15 chicken heart under open-circuit conditions. (f) ΔR of field potentials for E10 and E15 chicken hearts. ** $P < 0.01$. (g) ΔR of mechanical contractions for E10 and E15 chicken hearts. ** $P < 0.01$. (h) Latency time of E10 and E15 chicken hearts. All data are presented as mean ± SD ($n \geq 40$ cardiac cycles).

optical detection sensitivity. Whole embryonic chicken hearts were dissected from fertilized eggs incubated for 10 days and 15 days, corresponding approximately to HH35-36 and HH41-42, respectively[47] (“Methods”). After dissection and a 5 min-incubation in HEPES-buffered Tyrode’s solution, the hearts were directly interfaced with the PEDOT:PSS thin films and the laser beam was steered to the heart-polymer interface for optical recording (Fig. 4b). All recordings were performed under room temperature and open-circuit conditions without any electrodes.

Highly periodic signals were recorded for both embryonic day 10 (E10) and day 15 (E15) chicken hearts (Fig. 4c and d). The zoomed-in view (red dashed box) shows bioelectric signals from chicken hearts appear as sharp and fast spikes with a peak-to-peak rise time on the order of 13–20 ms. These bioelectric signals correspond to the field potentials of chicken hearts. Following the electrical signal spike is a slower baseline shift with complex shapes evolving over hundreds of milliseconds to a second. This corresponds to the mechanical contraction or beating of the chicken heart, known as the cardiac excitation-contraction coupling.[48] Because of the label-free nature of ECORE, we were able to perform long-term recording of chicken heart for over 10 minutes (Fig. 4e). To confirm the large baseline shift arises from the beating heart, we incubated the chicken heart with 0.2 mM blebbistatin before the measurement in a separate experiment. Blebbistatin is a potent myosin inhibitor that suppresses cardiomyocyte contraction without eliminating its action potential. Our recording showed that the slow baseline shifts gradually decrease, whereas the fast bioelectric spikes remain almost stable (Fig. S7).

Next, we characterized the amplitudes of the field potential and the mechanical signal, as well as the latency time, which is defined as the delay between the measured electrical activation and mechanical contraction (“Methods”). For E10 chicken hearts, the field potential shows a ΔR of $1.5 \times 10^{-4} \pm 6.7 \times 10^{-5}$ and increased to $5.1 \times 10^{-4} \pm 1.5 \times 10^{-4}$ for E15 chicken hearts ($P = 0.007$, Fig. 4f). The ΔR associated with mechanical contraction is approximately two orders of magnitude larger than the ΔR measured for field potentials, and increased from $24 \times 10^{-4} \pm 5.9 \times 10^{-4}$ to $160 \times 10^{-4} \pm 60 \times 10^{-4}$ for E10 and E15 chicken hearts ($P = 0.003$, Fig. 4g). We note the physical origins of ΔR are different for the field potentials and mechanical contractions. The field potential signal arises from the voltage-induced absorbance change of the PEDOT:PSS thin films due to electrochromism, whereas the slow mechanical contraction signal is due to the beating heart perturbing the optical interface between the tissue and the polymer surface. The ΔR of field potential can be converted into voltage by calibrating the PEDOT:PSS thin film using a 1 mV squarewave potential on top of a −100 mV bias potential (open-circuit potential when chicken heart was interfaced with the polymer film). The field potentials are 0.5 ± 0.2 mV and 1.5 ± 0.4 mV for E10 and E15 chicken hearts, respectively. The latency time of the heart is approximately 300 ms and remains unchanged for E10 and E15 chicken hearts ($P = 0.782$, Fig. 4h).

These results are consistent with the development of the chicken heart. E10 chicken heart is actively beating and structurally formed but remains immature and highly trabeculated. Continued development toward E15 leads to increased chamber organization, maturation of conduction pathways, and more coordinated contractile activity, resembling a mature heart.[49,50] The latency time between the two components remains unchanged, suggesting that the mechanical response is consistently triggered by electrical activation with a stable delay. We note the longer latency time measured here *ex vivo* compared to literature values likely reflects the slower development of detectable tissue motion at the heart-polymer interface, rather than at the single-cell level.

Discussion

In this work, we showed that introducing NaCl during EDOT electropolymerization in the presence of PSS can effectively tune the structure, electrochromic contrast and electrochemical behavior of PEDOT:PSS thin films, and at the same time maintain its biocompatibility. Incorporation of Cl^- as competing counterions during electropolymerization can modify the charge compensation environment and alters the organization of PEDOT within the PSS matrix. This leads to higher surface uniformity and optical anisotropy, but reduced conjugation length and electrochemical active site concentration.

The structural change results in a shift in the electrochromic response of PEDOT:PSS thin films, manifested by the blue-shifted Vis-NIR spectroelectrochemistry with increasing NaCl concentration. The π–π* absorption peak, polaron and bipolaron transition wavelengths, and isosbestic point shifts across a 120 nm range. We have shown the rate of voltage-dependent absorbance change at specific wavelengths is directly related to the ECORE detection sensitivity. Therefore, the ECORE detection sensitivity can be maximized by matching the PEDOT:PSS electropolymerization conditions with the probing laser wavelength (Fig. S1). Moreover, at shorter wavelengths (*e.g.*, $\leq$561 nm) the film absorbance decreases with voltages, whereas at longer wavelengths (*e.g.*, $\geq$658 nm), the film absorbance increases with voltages. Precisely tuning the isosbestic point wavelength will further allow ECORE measurements with multiple probing wavelengths for noise and motion artifacts rejection.[17] In addition, the ECORE optical response exhibits polarization dependences that become more pronounced with Cl^- incorporation into the PEDOT:PSS film. This could be due to the optical anisotropy in conjugated polymer films, which increases as Cl^- alters PEDOT organization in the PSS matrix. The degree of polarization dependence is also strongly coupled to the bias potential applied to the film. This may be attributed to differences in PEDOT chain conformation associated with the benzoid (reduced) and quinoid (oxidized) electronic structures.[51,52]

Tuning PEDOT:PSS thin film spectra using NaCl keeps the biocompatibility of PEDOT:PSS thin films. We further established embryonic chicken hearts at different developmental stages as a reliable model system to study bioelectric signals. We resolved both the spontaneous field potential and the resulting mechanical contraction of the chicken heart. Quantitative analysis shows

that both electrical and mechanical signal amplitudes increase from embryonic day 10 to day 15, whereas the latency time remains unchanged. This is consistent with the maturation stages of the embryonic chicken heart. The capability to simultaneously record electrical and mechanical signals, and perform long-term recordings highlights ECORE as a label-free platform for probing complex cardiac physiological dynamics in a non-perturbative manner.

ECORE uses PEDOT:PSS thin films to convert bioelectric potentials into optical readouts *via* electrochromism, rather than fluorescence. In its current form, ECORE is primarily used for label-free optical recording of extracellular field potentials and does not provide the capability for target-specific biochemical sensing. Looking forward, understanding the design rules of electrochromic polymers for ECORE, such as how backbone and side-chain chemistries, and how film microstructures influence ion-driven electrochromic responses in biological systems will further optimize the ECORE performance. Integrating ECORE with biointerfaces functionalized with selective molecular recognition motifs could also enable label-free optical detection of specific biochemical targets.

Methods

Device fabrication, electropolymerization and spin coating

Indium tin oxide (ITO)-coated glass slides (25 × 25 × 0.4 mm^3, sheet resistance R_s = 70–100 Ω, Surplus Part No. X260, Delta Technologies) were sequentially cleaned by sonication in dish soap water for 5 min, acetone (Fisher Chemical) for 15 min, and isopropyl alcohol (Macron Fine Chemicals) for 15 min. The substrates were dried under a stream of air and further treated using either a UV-ozone cleaner (low-pressure Hg lamp, BHK Inc.) for (4 min) or a plasma cleaner (PDC-32G, Harrick Plasma) at medium power for 4 min. Custom 3D-printed poly(lactic acid) (PLA) sample wells with a circular bottom opening (Ø6 mm) were attached to the ITO substrates using silicone adhesive (RTV108, Momentive) and cured for at least 6 h prior to use.

A total of 20 mL aqueous solution was prepared by dissolving 0.4 g poly(sodium 4-styrenesulfonate) (PSS, M_W = 70 kDa, Sigma-Aldrich) in Milli-Q water (2 wt%), followed by the addition of 20 μL 3,4-ethylenedioxythiophene (EDOT, Sigma-Aldrich) to obtain a 10 mM solution. For molecular weight studies, PSS with M_w = 3400 Da and 15 000 Da (Agilent Technologies) was used. For dopant studies, NaCl (Sigma-Aldrich) was added to achieve the desired concentration, and for pH-dependent studies, the solution pH was adjusted using H_2SO_4 (J.T. Baker) or NaOH (Sigma-Aldrich) to avoid introducing other competing counterions. The solution was equilibrated overnight and filtered through a 1.2 μm syringe filter (Sartorius) prior to use. A volume of 1 mL of the filtered solution was added to the sample well, and electropolymerization was carried out under a constant current of 100 μA using a potentiostat (SP-150e, BioLogic) in a three-electrode configuration, resulting in PEDOT:PSS thin films with an area of ~28.3 mm^2 on the ITO substrates. The film thickness was controlled by varying the electrodeposition time.

For spin-coated PEDOT:PSS films, a dispersion consisting of 16 mL PEDOT:PSS (Clevios PH1000, Heraeus), 4 mL ethylene glycol (Sigma-Aldrich), 24 μL sodium dodecylbenzenesulfonate (Tokyo Chemical Industry Co., Ltd), and 200 μL (3-glycidyloxypropyl)trimethoxysilane (Sigma-Aldrich) was prepared by vortex mixing followed by sonication for 5 min and filtration through a 1.2 μm cellulose acetate syringe filter (add vendor here). The dispersion was spin-coated onto ITO substrates at 5500 rpm using a static dispense method and annealed at 140 °C for at least 1 h. Prior to measurements, all spin-coated films were electrochemically pre-conditioned by cycling the potential between −0.3 V and 0.3 V at a scan rate of 100 mV s^{-1} for 5 cycles in HEPES (4-(2-hydroxyethyl)−1-piperazineethanesulfonic acid)-buffered Tyrode's solution (1 mL 1 M $CaCl_2$, 500 μL 1 M $MgCl_2$, 5 mL HEPES stock (1 M) (Gibco, Thermo Fisher), 4.237 g NaCl (145 mM), 149 mg KCl (4 mM), 500 mL Milli-Q water. The pH of the HEPES-buffered Tyrode's solution is adjusted to 7.4 using NaOH.

UV-Vis-NIR spectroelectrochemistry

A polymer thin-film sample coated on ITO glass, an Ag/AgCl reference electrode (RE-6, BASi Research Products), and a platinum counter electrode were placed in a custom-designed 3D-printed cuvette and positioned in the sample chamber of a UV-vis-NIR spectrophotometer (Cary 60 UV-Vis, Agilent). The cuvette position was adjusted such that the probing light beam passed through the center of the polymer film. The UV-vis-NIR spectrophotometer scanned from 1100 to 300 nm with a 1 nm step size. HEPES-buffered Tyrode's solution was used as the aqueous electrolyte for all measurements. A potentiostat (SP-150e, BioLogic) was used to apply potentials to the polymer films from +600 mV to −900 mV in 100 mV steps. To directly compare the UV-vis-NIR spectroelectrochemical shifts of all polymers at specific probing laser wavelengths, the polymer film absorbance was normalized with respect to the peak absorbance value in the reduced state at an applied voltage of −900 mV.

Film thickness measurements

A razor blade was used to gently scratch near the center of the polymer thin films. The thickness of the polymer thin films was then measured using a Dektak3ST profilometer (Sloan). For each sample, at least three measurements were performed, and the average film thickness was calculated.

Atomic force microscopy (AFM)

AFM was used to characterize morphology of PEDOT:PSS films. Surface topography was acquired in tapping mode using a MFP-3D AFM (Asylum Research) with Tap300Al-G probes (BudgetSenors). All images were collected at a scan rate of 1 Hz with 256 × 256 pixels. Surface roughness was calculated using the Asylum Research AFM software. Images were processed with Gwyddion. Grain size statistics, 2D FFT and PSDF were carried out with Gwyddion.

Coloration of PEDOT:PSS polymer thin films

The color change of all polymer thin films was captured using a digital camera (EOS R5, Canon) under identical light conditions

in a photo studio light box. All images were processed using the same parameters in Adobe Lightroom. A potentiostat (SP-150e, BioLogic) was used to apply different potentials to the polymer films. The aqueous electrolyte used for all measurements was HEPES-buffered Tyrode's solution.

X-ray photoelectron spectroscopy (XPS)

XPS measurements were performed using a Kratos Axis Supra+ photoelectron spectrometer equipped with a monochromatic Al Kα X-ray source (1486.7 eV) at a 90° emission collection angle. High-resolution spectra were acquired with a step size of 0.1 eV. The C 1s peak at 284.8 eV was used as the reference for charge correction. Measurements were conducted within two days of material synthesis to minimize oxidation of the samples. Data was analyzed using CasaXPS software. A Shirley background was applied to all spectra, and peaks were fitted using a Gaussian–Lorentzian mixed line shape (GL30). Both S 2p and Cl 2p doublets were fitted with the constraints that the FWHM values of the $2p_{3/2}$ and $2p_{1/2}$ peaks were identical, the peak area ratio was fixed at 2 : 1 ($2p_{3/2}$: $2p_{1/2}$), and the spin–orbit splitting was set to 1.18 eV for S and 1.60 eV for Cl.

Attenuated total reflectance-Fourier transform infrared (ATR-FTIR) spectroscopy

ATR-FTIR spectroscopy was performed using a Thermo Nicolet iS50 FTIR. The polymer film on an ITO glass was pressed directly onto the ATR crystal for data collection. All spectra were collected in absorbance mode using 64 scans at a resolution of 4 cm^{-1} over the range of 4000–400 cm^{-1}. We note the ITO substrate exhibits strong absorbance in the 1500–500 cm^{-1} range, which slightly weakens characteristic peaks of PEDOT:PSS.

Multilayer reflectance modeling

The optical response of the multilayer thin-film system was modeled using a transfer-matrix method described in detail before[16] implemented in a custom Python script. In brief, the structure was represented as a stack of BK7 glass/ITO/PEDOT:PSS/water, where each layer was defined by its complex refractive index and thickness. For each incident angle, the propagation angle in each layer was determined using Snell's law, and the phase accumulation was calculated from the *z*-component of the wavevector. Fresnel reflection coefficients were computed at each interface, and the total reflectivity was obtained from the resulting transfer matrix.

Simulations were performed at a wavelength of 561 nm to match the probing laser used in experiments. The calculated angle-dependent reflectivity was used to interpret the film reflectance change, ΔR, measured in experiments. Fitting of experimental data was carried out by comparing simulated reflectivity with experimentally measured ΔR using a custom Python optimization routine. Parameters including PEDOT:PSS film thickness, complex refractive indices, and angular offset were adjusted to minimize the squared residuals between simulation and experiment.

Electrochemical characterization

Cyclic voltammetry (CV) measurements of PEDOT:PSS thin films were performed using a potentiostat (SP-150e, BioLogic) in a three electrode configuration. The ITO glass served as the working electrode with an Ag/AgCl reference electrode (RE-6, BASi Research Products) and a platinum counter electrode. All measurements were carried out in HEPES-buffered Tyrode's solution. The potential was swept between +600 mV and −900 mV at a scan rate of 100 mV s^{-1}. Each sample was cycled for five consecutive scans, and the data from the final cycle were used to ensure stable electrochemical response. The electroactive site concentration, which reflects the density of redox-accessible PEDOT units, was quantified by integrating the cathodic charge (reductive current) from the CV curves.

Embryonic chicken heart isolation

Embryonic chicken hearts were isolated from fertilized eggs (University of Illinois Feed Technology Center) incubated for 10 or 15 days using an egg incubator. All visible blood vessels were carefully removed using fine tweezers under a dissection microscope in a cardioplegic solution (13.44 mM KCl, 12.6 mM $NaHCO_3$, 280 mM glucose, 34 mM mannitol). The isolated hearts were then incubated in the same cardioplegic buffer at 37 °C for 5 min prior to ECORE measurements.

Optical setup

A fiber-coupled 561 nm diode-pumped solid-state laser (Excelsior, Spectra-Physics) was collimated using an aspheric lens (C280TMD-A, Thorlabs) mounted in a Z-adjustable mount (SM1ZA, Thorlabs) and directed through a 1.0 (10%) neutral density filter (NE10A, Thorlabs). The polarization of the collimated beam was then adjusted using a half-wave plate (WPH05M-561, Thorlabs) and filtered by a polarizing beam splitter cube (PBS201, Thorlabs), where the rejected beam was directed to a beam dump. The transmitted beam was directed through a series of lenses and mirrors and subsequently split by a second polarizing beam splitter cube into a sample beam and a reference beam. The polarization of the probing beam was further adjusted using additional half-wave plates to control the *p*- and *s*-polarization components. The sample beam was coupled to the device using a 20 mm right-angle BK-7 prism (PS908, Thorlabs) mounted on a rotational stage (CR1, Thorlabs). The laser incident angle was tuned by adjusting the prism orientation. The rotational stage was mounted on an XYZ linear translational stage (9064-XYZ, Newport), allowing precise positioning of the prism. The reflected sample beam and the reference beam were directed to a home-made differential photodetector. The probing laser spot size, D, defined as $D = 2 \times \mathrm{FWHM}/\sqrt{(2\ln 2)}$, where FWHM is the full-width-at-half-maximum of the measured laser spot intensity profile, was determined to be ∼30 μm. More details regarding the optical setup were described in our previous work.[16–18]

ECORE data acquisition

For squarewave measurements, a three-electrode configuration was employed as previously described. A 1 Hz, 1 mV square-wave

potential at different bias potentials was applied using a potentiostat (SP-150e, BioLogic). A thin layer of Type F immersion oil (n_0 = 1.518, Leica) was applied to the bottom of the device to achieve refractive index matching with the prism and to suppress back reflection from the ITO substrate.

For recording of isolated embryonic chicken hearts, the polymer films were used directly without any additional treatment. The isolated chicken heart was transferred onto the polymer film immediately after incubation. A limited amount (20–40 μL) HEPES-buffered Tyrode's solution pre-warmed to 37 °C was added to the device to prevent the heart from floating. The heart formed good contact with the polymer film and maintained spontaneous beating for up to 1 h. The 561 nm probing laser was focused on the location of interest on the isolated chicken heart. The sample and the reference beams were directed to the two photodiodes of the homemade differential photodiode detector, which convert optical signals from the probing laser into voltage signals. The voltage output from the differential photodetectors was amplified through a low-noise voltage preamplifier (SR560, Stanford Research Systems) with a built-in 1 kHz internal low pass filter to remove the amplifier noise. The filtered, amplified signal was then digitized at 10 kHz rate using a low-noise digitizer (Axon Digidata 1550 B, Molecular Devices) and recorded using the Clampex software. The light intensities of the sample beam and the reference beam reaching the differential photodetectors were manually adjusted by rotating a halfwave plate in the light path. The differential photodetector was therefore ''balanced'' to maximize the recording dynamic range for reflectance change ΔR (in Volts). The probing laser beam power (in mV) was measured using a photodiode power sensor (S121C, Thorlabs) connected to an optical power meter (PM100D, Thorlabs).

Data analysis

The reflectance change ΔR (in Volts) was normalized by the incident probing laser power, P_{in}, defined as:

$$\Delta R = \frac{\text{recorded signal amplitude[V]}}{\text{responsivity [A W}^{-1}\text{]} \times \text{feedback resistance [}\Omega\text{]} \times P_{in}\text{[W]} \times \text{amplification}}$$

The responsivity of the silicon photodiode (FDS100, Thorlabs) at 561 nm is 0.232 A W^{-1}. The feedback resistance of the differential photodetector is 100 kΩ. The amplifier gain was set to 50× for square-wave characterizations and 10× or 5× (depending on the signal amplitude) for isolated chicken heart recordings.

For squarewave potentials, electrical noise at 60 Hz was removed using electrical noise filters implemented in Clampfit 11 (Molecular Devices). The signals were then processed in Python using a first-order Butterworth high-pass filter (cutoff frequency 0.2 Hz) to remove baseline drift and a third-order Butterworth low-pass filter (cutoff frequency 500 Hz) to remove high-frequency noise. Custom Python scripts were used to extract ΔR from the filtered signals. The ΔR of squarewave recordings was determined as the average step height between consecutive high and low states over a recording duration of 120 s (≥110 cycles). To ensure statistical robustness and sufficient sampling of the periodic responses, the extracted waveforms were analyzed using an unsupervised clustering approach. Each waveform was centered and described by statistical features including its amplitude and shape, followed by density-based spatial clustering (DBSCAN) to separate valid signal traces from noise. Each dataset contains at least 40 valid squarewaves cycles and was used to calculate the average ΔR and standard deviation.

For embryonic chicken heart recordings, the same filtering procedure was applied, including 60 Hz electrical noise filters in Clampfit 11 followed by high-pass (0.1 Hz) and low-pass (500 Hz) Butterworth filters in Python. The electrical and mechanical components of the recording traces were analyzed using the same processing framework as squarewave potentials. Mechanical signals were first identified from the filtered traces as local extrema, and their onset times were determined from the left intersection of the waveform width at a defined relative height. Electrical spikes preceding each mechanical event were then identified within a defined temporal search window, and the electrical onset was determined using a slope-based criterion. The amplitudes of both electrical and mechanical signals were calculated as the difference between the signal extremum (peak or trough) and the corresponding onset baseline. The latency between the two peaks was determined as the time difference between the electrical onset and the mechanical onset. Only events with valid electrical-mechanical pairing were retained. For each recording (typically 200–400 s in duration, depending on the beating frequency), at least 50 consecutive paired events were required to ensure reliable statistical analysis. Mean values and standard deviations were then calculated from these events.

Conflicts of interest

There are no conflicts of interest to declare.

Data availability

All data supporting the findings of this study are available within the article and its supplementary information (SI) files. Any additional requests for information can be directed to, and will be fulfilled by, the corresponding author. Supplementary information is available. See DOI: https://doi.org/10.1039/d6tb00816j.

Acknowledgements

The authors thank Professor Ying Diao for the access of the UV-Vis-NIR spectrophotometer in her lab and Priyotosh Bairagya

for helping with the UV-Vis-NIR spectrophotometer training. This work was supported by the American Heart Association Career Development Award (https://doi.org/10.58275/AHA.25CDA1436867.pc.gr.229603) and the Roy J. Carver Charitable Trust Individual Investigator Award. This work was carried out in part in the Materials Research Laboratory Central Research Facilities, University of Illinois.

References

1 B. P. Bean, The action potential in mammalian central neurons, *Nat. Rev. Neurosci.*, 2007, **8**, 451–465.
2 J. M. Nerbonne and R. S. Kass, Molecular Physiology of Cardiac Repolarization, *Physiol. Rev.*, 2005, **85**, 1205–1253.
3 D. J. Blackiston, K. A. McLaughlin and M. Levin, Bioelectric controls of cell proliferation: ion channels, membrane voltage and the cell cycle, *Cell Cycle*, 2009, **8**, 3527–3536.
4 J. Grune, M. Yamazoe and M. Nahrendorf, Electroimmunology and cardiac arrhythmia, *Nat. Rev. Cardiol.*, 2021, **18**, 547–564.
5 M. Levin, Bioelectric signaling: Reprogrammable circuits underlying embryogenesis, regeneration, and cancer, *Cell*, 2021, **184**, 1971–1989.
6 R. Feiner and T. Dvir, Tissue–electronics interfaces: from implantable devices to engineered tissues, *Nat. Rev. Mater.*, 2017, **3**, 17076.
7 O. Bettucci, G. M. Matrone and F. Santoro, Conductive Polymer-Based Bioelectronic Platforms toward Sustainable and Biointegrated Devices: A Journey from Skin to Brain across Human Body Interfaces, *Adv. Mater. Technol.*, 2022, **7**, 2100293.
8 J. Zhang, Z. Cheng, P. Li and B. Tian, Materials and device strategies to enhance spatiotemporal resolution in bioelectronics, *Nat. Rev. Mater.*, 2025, **10**, 425–448.
9 T. Knöpfel and C. Song, Optical voltage imaging in neurons: moving from technology development to practical tool, *Nat. Rev. Neurosci.*, 2019, **20**, 719–727.
10 P. Liu and E. W. Miller, Electrophysiology, Unplugged: Imaging Membrane Potential with Fluorescent Indicators, *Acc. Chem. Res.*, 2019, **53**(1), 11–19.
11 M. Z. Lin and M. J. Schnitzer, Genetically encoded indicators of neuronal activity, *Nat. Neurosci.*, 2016, **19**, 1142–1153.
12 Y. Bando, M. Sakamoto, S. Kim, I. Ayzenshtat and R. Yuste, Comparative Evaluation of Genetically Encoded Voltage Indicators, *Cell Rep.*, 2019, **26**, 802–813.e4.
13 S. Mennerick, *et al.*, Diverse voltage-sensitive dyes modulate GABAA receptor function, *J. Neurosci.*, 2010, **30**, 2871–2879.
14 T. H. Grandy, S. A. Greenfield and I. M. Devonshire, An evaluation of in vivo voltage-sensitive dyes: pharmacological side effects and signal-to-noise ratios after effective removal of brain-pulsation artifacts, *J. Neurophysiol.*, 2012, **108**, 2931–2945.
15 Y. Zhou, E. Liu, H. Müller and B. Cui, Optical Electrophysiology: Toward the Goal of Label-Free Voltage Imaging, *J. Am. Chem. Soc.*, 2021, **143**, 10482–10499.
16 F. S. Alfonso, *et al.*, Label-free optical detection of bioelectric potentials using electrochromic thin films, *Proc. Natl. Acad. Sci. U. S. A.*, 2020, **117**, 17260–17268.
17 Y. Zhou, *et al.*, Dual-Color Optical Recording of Bioelectric Potentials by Polymer Electrochromism, *J. Am. Chem. Soc.*, 2022, **144**, 23505–23515.
18 Y. Zhou, *et al.*, Ultrasensitive label-free optical recording of bioelectric potentials using dioxythiophene-based electrochromic polymers, *Nat. Commun.*, 2025, **16**, 6776.
19 H. Jürgen, A. Rasche, A. Markus Pagels and B. Geschke, On the Origin of the So-Called Nucleation Loop during Electropolymerization of Conducting Polymers, *J. Phys. Chem. B*, 2007, **111**, 989–997.
20 H. Mousavi, L. M. Ferrari, A. Whiteley and E. Ismailova, Kinetics and Physicochemical Characteristics of Electrodeposited PEDOT:PSS Thin Film Growth, *Adv. Electron. Mater.*, 2023, **9**, 2201282.
21 B. D. Paulsen, K. Tybrandt, E. Stavrinidou and J. Rivnay, Organic mixed ionic–electronic conductors, *Nat. Mater.*, 2019, **19**, 13–26.
22 Y. Shin, *et al.*, Array-wide uniform PEDOT:PSS electroplating from potentiostatic deposition, *Biosens. Bioelectron.*, 2024, **261**, 116418.
23 T. Niederhoffer, A. Vanhoestenberghe and H. T. Lancashire, Methods of poly(3,4)-ethylenedioxithiophene (PEDOT) electrodeposition on metal electrodes for neural stimulation and recording, *J. Neural Eng.*, 2023, **20**(1), 011002.
24 J. E. Chung, *et al.*, High-Density, Long-Lasting, and Multi-region Electrophysiological Recordings Using Polymer Electrode Arrays, *Neuron*, 2019, **101**, 21–31.e5.
25 Y. Xiao, *et al.*, Electrochemical polymerization of poly(hydroxymethylated-3,4-ethylenedioxythiophene) (PEDOT-MeOH) on multichannel neural probes, *Sens. Actuators, B*, 2004, **99**, 437–443.
26 P. Tehrani, *et al.*, The effect of pH on the electrochemical over-oxidation in PEDOT:PSS films, *Solid State Ionics*, 2007, **177**, 3521–3527.
27 E. Poverenov, M. Li, A. Bitler and M. Bendikov, Major Effect of Electropolymerization Solvent on Morphology and Electrochromic Properties of PEDOT Films, *Chem. Mater.*, 2010, **22**, 4019–4025.
28 V. Kabanova, O. Gribkova and A. Nekrasov, Poly(3,4-ethylenedioxythiophene) Electrosynthesis in the Presence of Mixtures of Flexible-Chain and Rigid-Chain Polyelectrolytes, *Polymers*, 2021, **13**, 3866.
29 U. Lang, E. Müller, N. Naujoks and J. Dual, Microscopical Investigations of PEDOT:PSS Thin Films, *Adv. Funct. Mater.*, 2009, **19**, 1215–1220.
30 T. Takano, H. Masunaga, A. Fujiwara, H. Okuzaki and T. Sasaki, PEDOT Nanocrystal in Highly Conductive PEDOT:PSS Polymer Films, *Macromolecules*, 2012, **45**(9), 3859–3865.
31 A. V. Volkov, *et al.*, Understanding the Capacitance of PEDOT:PSS, *Adv. Funct. Mater.*, 2017, **27**, 1700329.
32 A. P. Nowak, M. Wilamowska and A. Lisowska-Oleksiak, Spectroelectrochemical characteristics of poly(3,4-ethylenedioxythiophene)/iron hexacyanoferrate film-modified electrodes, *J. Solid State Electrochem.*, 2009, **14**, 263–270.
33 J. L. Brédas, Relationship between band gap and bond length alternation in organic conjugated polymers, *J. Chem. Phys.*, 1985, **82**, 3808–3811.

34 J. J. Apperloo, *et al.*, Optical and redox properties of a series of 3,4-ethylenedioxythiophene oligomers, *Chemistry*, 2002, **8**, 2384–2396.
35 D. Kim, J. F. Franco-Gonzalez and I. Zozoulenko, How Long are Polymer Chains in Poly(3,4-ethylenedioxythiophene):Tosylate Films? An Insight from Molecular Dynamics Simulations, *J. Phys. Chem. B*, 2021, **125**(36), 10324–10334.
36 I. Zozoulenko, *et al.*, Polarons, Bipolarons, And Absorption Spectroscopy of PEDOT, *ACS Appl. Polym. Mater.*, 2018, **1**(1), 83–94.
37 L. Groenendaal, F. Jonas, D. Freitag, H. Pielartzik and J. R. Reynolds, Poly(3,4-ethylenedioxythiophene) and Its Derivatives: Past, Present, and Future, *Adv. Mater.*, 2000, **12**, 481–494.
38 J. Lee, *et al.*, Influence of Channel Thickness and Counter-ion Composition on the Performance and Stability of Interdigitated Organic Electrochemical Transistors (OECTs) Using Electrochemically Deposited PEDOT, *ACS Appl. Electron. Mater.*, 2025, **7**(18), 8440–8455.
39 V. Subramanian and D. C. Martin, In Situ Observations of Nanofibril Nucleation and Growth during the Electrochemical Polymerization of Poly(3,4-ethylenedioxythiophene) Using Liquid-Phase Transmission Electron Microscopy, *Nano Lett.*, 2021, **21**(21), 9077–9084.
40 V. Subramanian and D. C. Martin, Direct Observation of Liquid-to-Solid Phase Transformations during the Electrochemical Deposition of Poly(3,4-ethylenedioxythiophene) (PEDOT) by Liquid-Phase Transmission Electron Microscopy (LPTEM), *Macromolecules*, 2021, **54**(14), 6956–6967.
41 Y. Mochizuki, T. Horii and H. Okuzaki, Effect of pH on Structure and Conductivity of PEDOT/PSS, *Trans. Mater. Res. Soc. Jpn.*, 2012, **37**, 307–310.
42 M. J. Walter and J. M. Lupton, Unraveling the inhomogeneously broadened absorption spectrum of conjugated polymers by single-molecule light-harvesting action spectroscopy, *Phys. Rev. Lett.*, 2009, **103**, 167401.
43 Y. Xia and J. Ouyang, Salt-Induced Charge Screening and Significant Conductivity Enhancement of Conducting Poly-(3,4-ethylenedioxythiophene):Poly(styrenesulfonate, *Macromolecules*, 2009, **42**, 4141–4147, DOI: 10.1021/ma900327d.
44 P. C. Hobbs, Ultrasensitive laser measurements without tears, *Appl. Opt.*, 1997, **36**, 903–920.
45 M. Kong, M. Garriga, J. S. Reparaz and M. I. Alonso, Advanced Optical Characterization of PEDOT:PSS by Combining Spectroscopic Ellipsometry and Raman Scattering, *ACS Omega*, 2022, **7**(43), 39429–39436.
46 C. Dingler, R. Walter, B. Gompf and S. Ludwigs, In Situ Monitoring of Optical Constants, Conductivity, and Swelling of PEDOT:PSS from Doped to the Fully Neutral State, *Macromolecules*, 2022, **55**(5), 1600–1608.
47 V. Hamburger and H. L. Hamilton, A series of normal stages in the development of the chick embryo, *J. Morphol.*, 1951, **88**, 49–92.
48 D. M. Bers, Cardiac excitation–contraction coupling, *Nature*, 2002, **415**, 198–205.
49 J. G. Wittig and A. Münsterberg, The Chicken as a Model Organism to Study Heart Development, *Cold Spring Harbor Perspect. Biol.*, 2020, **12**, a037218.
50 V. Olejnickova, *et al.*, Development of ventricular trabeculae affects electrical conduction in the early endothermic heart, *Dev. Dyn.*, 2024, **253**, 78–90.
51 J. Ouyang, *et al.*, On the mechanism of conductivity enhancement in poly(3,4-ethylenedioxythiophene):poly(styrene sulfonate) film through solvent treatment, *Polymer*, 2004, **45**, 8443–8450.
52 N. A. Shahrim, Z. Ahmad, A. W. Azman, Y. F. Buys and N. Sarifuddin, Mechanisms for doped PEDOT:PSS electrical conductivity improvement, *Mater. Adv.*, 2021, **2**, 7118–7138.